

Bernhard Huber^{1,*}
Georg Johann Krebs²
Lingga Aksara Putra¹
Matthias Gaderer¹


Positioning a Measurement System for Determining the Mixing Quality in Biogas Digesters

Mixing quality in agricultural biogas plants is crucial for nutrition supply to the microorganisms and needs to be ensured by an energy-efficient mixing strategy. Various approaches have been proposed to determine the mixing quality in biogas digesters. Among them are magnetic-inductive or force sensors brought into vertical digesters through the concrete wall. This article presents an approach to locating these sensors effectively around the circumference of the digester to avoid positioning in dead zones and maximize information quality regarding flow and mixing behavior. Particle image velocimetry is used to measure flow fields in a transparent model digester. Finally, optimum measurement locations considering three widely used agitator geometries are suggested.

Keywords: Biogas digester, Dimensional analysis, Mixing quality, Particle image velocimetry

Received: May 15, 2023; *revised:* July 10, 2023; *accepted:* July 24, 2023

DOI: 10.1002/ceat.202300241

 This is an open access article under the terms of the Creative Commons Attribution-NonCommercial-NoDerivs License, which permits use and distribution in any medium, provided the original work is properly cited, the use is non-commercial and no modifications or adaptations are made.



Supporting Information
available online

1 Introduction

To mitigate the impacts of climate change, the Paris Agreement of 2015 aims to limit the increase in the global average temperature to 1.5 °C compared to the pre-industrial level. Contributing to this task, the German government has formulated the goal of carbon dioxide neutrality by the year 2045 [1]. Limits for annual emission amounts for the sectors of energy industry, industry, traffic, agriculture, waste industry, and others have been set. Enhanced use of renewable energy sources is necessary to meet these emission reduction goals.

By 2020, more than 9600 biogas plants have been installed in Germany, supplying an installed electric power of almost 5800 MW [2]. Up to 90 % of these plants are built as continuously stirred tank reactors (CSTRs) using mechanical mixing equipment [3]. Energy use for the plant supply accounts for an average of about 8 % of the electric energy produced by the plant. A relatively large percentage of up to 50 % of that amount is used for mixing [4, 5].


Approaches for getting insight into the mixing quality of biogas digesters can be divided into local and global measurement systems. Global measurements like particle image velocimetry (PIV) [6], planar laser-induced fluorescence (PLIF), and electrical resistance thermometry (ERT) [7] are mainly applied in laboratory-scale test rigs, whereas local measurement techniques (i.e., pressure, pH, conductivity, temperature, reflected light sensors) can be implemented in real-scale plants [8].

Tab. 1 lists several developments for the online measurement of digester content properties and flow quantities. Ion-selective electrodes were calibrated to estimate chemical oxygen demand and volatile fatty acid concentration [9]. An in-line tube viscometer was developed by Mönch-Tegeeder et al. [10], which

measures the pressure drop of the digester content pumped through an external pipe to calculate the apparent viscosity. Single-point measurements with the technologies presented in [9] and [10] give information about biological and rheological properties but do not directly indicate the mixing quality.

Several concepts like bending beam [11], magnet-induced [12], and ultrasonic-based anemometry [13] have been examined to estimate the local flow velocity at the installation position. Nsair et al. [11] used a strain gauge applied on an aluminum rod which was introduced orthogonal into the flow through the digester wall. It was tested at various positions around the circumference of the digester at different heights and depths to prove its robustness. The signal of this so-called bending beam sensor was correlated to the local flow velocity. Another way of measuring flow velocities in real biogas plants by inserting a magnet-induced sensor was reported by Kress et al. [12]. The sensor was induced through the concrete ceiling of the digester at various positions on the centerline. Average flow velocity and the velocity range were investigated to analyze the influence of varying dry matter content and viscosity.

¹Bernhard Huber
(b.huber@tum.de),

Lingga Aksara Putra  <https://orcid.org/0000-0001-6321-9139>,
Prof. Dr.-Ing. Matthias Gaderer

Technical University of Munich, Campus Straubing for Biotechnology and Sustainability, Schulgasse 16, 94315 Straubing, Germany.

²Georg Johann Krebs
Ostbayerische Technische Hochschule Regensburg, Fakultät Maschinenbau, Galgenbergstr. 30, 93053 Regensburg, Germany.

Table 1. Overview of developments in the field of online-monitoring digester content properties and mixing quality.

Technology	Measured parameter	Estimated/calculated parameter	Type of parameter local/global	Year	Ref.
Ion-selective electrodes	Voltage	Chemical oxygen demand, volatile fatty acid content	Local	2010	[9]
In-line viscometer	Pressure difference	Apparent viscosity	Local fluid property	2015	[10]
Bending beam sensor	Force	Flow velocity	Local	2018	[11]
Magnet-induced sensor	Induced current	Flow velocity	Local	2020	[12]
Ultrasonic-based anemometer	By particles reflected sound profile	Flow velocity	Local	2021	[13]
PIV	Particle displacement	Surface velocity	Local, due to the limited field of view	2021	[13]
Wireless sensor network with sensor balls and position tracking system	Pressure, temperature, acceleration, rotation rate, magnetometer		Global	2021	[14]

Even PIV was suggested to determine the surface velocity of the moving digester content [13]. Nevertheless, it remains limited to measurements on the fluid surface inside the digester due to the necessity of transparent fluids for measurements on deeper layers.

Buntkiel et al. [14] proposed a swarm of sensor balls equipped with a tracking system to measure various quantities along streamlines in the biogas digester. As these sensor balls travel with the flow through the digester, it is considered a global online-measurement technique here.

While the presented studies [11–13] use local point measurements, the relevance of the measurement positions for determining global flow field parameters is not discussed. Answering that question will provide more information about the flow field and enable a reduction of necessary measurement positions.

According to Jobst et al. [15], a flow velocity of around 0.05 m s^{-1} supports mass transfer during hydrolysis and acidification processes. However, Kress et al. [10] did not confirm this effect in their full-scale study, where the agitation time was reduced from 20 to 4 min an hour, and the biogas production was not affected negatively. Furthermore, Kress et al. [12] reported that for the mentioned range of dry matter content even flow speeds below 0.025 m s^{-1} in the horizontal direction did show a certain level of nutrient distribution and mixing quality. One restriction of that statement is that only horizontal velocities were measured. Other effects of nutrient distribution, like diffusion or mixing by rising gas bubbles, might also be present.

Considering the need to quantify the mixing quality in biogas plants, cost-effective and reliable measurement solutions must be developed. Installation positions around the circumference of a CSTR below the liquid level are especially suitable because the presence of an explosive atmosphere is unlikely. Accordingly, the need for electronic equipment suitable for explosion zones is avoided.

That work aims to find positions for local flow sensors around the circumference of a biogas digester with maximum

information output. Therefore, experiments have been done with three different agitator geometries at various rotational speeds and viscosities of the transparent model fluid in a lab-scale trial plant. The average velocity fields on various horizontal layers of the model digester are derived from PIV measurements. Analyzing the data leads to proposals for optimum positions of flow sensors to monitor the mixing process.

2 Methods

Addressing the formulated question, a scaled-down, transparent model digester with a transparent model fluid is designed through dimensional analysis. The velocity vector fields in various horizontal layers of the digester are measured via PIV.

The design of the experimental setup is based on a survey among 345 biogas plant owners in Germany published by Fachagentur Nachwachsende Rohstoffe e. V. (FNR). Around 90 % of the investigated biogas plants in the Biogas-Messprogramm III (BMP III) are equipped with a CSTR. A majority of 59 % state that a propeller agitator is used in their plant. The second most significant share is held by the long-axis agitator, which is used by 37 % of the investigated plants [16]. Therefore, this study uses a CSTR. The propeller and long-axis agitator are used to address the mixing configuration of the majority of plants. However, the concept of the paddle agitator is investigated as an alternative concept of mixing technology in biogas plants.

Around 60 % of the biogas plants investigated in the BMP III show dry matter contents between 8 to 12 %, and 51 % of plants participating in the operator survey are run in the mesophilic temperature range ($35\text{--}42^\circ\text{C}$) [16]. In this study, the viscosity is modeled according to literature data for digester content of 8 % dry matter (DM) with a 0.8 % carboxymethyl cellulose (CMC)/water mixture (Tab. 3). For the long-axis and paddle agitator, a second thickened mixture with 0.9 % CMC-content is considered.

The nominal rotational speed in the experiments was varied between 1000–2000 min^{-1} for the propeller, 400–700 min^{-1} for the long axis agitator, and 100–250 min^{-1} for the paddle agitator. This corresponds to a maximum of -53% and $+15\%$ compared to the nominal speed. The variation is limited by the excessive suction of air bubbles into the model fluid at higher rotational speeds and low fluid movement at lower rotational speeds.

2.1 Dimensional Analysis

To ensure similarity between the original and model according to the Buckingham Π -theorem [17], three relevant key figures are considered for the design of the trial plant: Newton number Ne (Eq. (1)), Reynolds number Re (Eq. (2)), and the ratio Q (Eq. (3)) of shear rate to rotational speed [18]. This approach is based on Annas et al. [18], whose proposal extends the concept of Böhme and Stenger [19].

$$Ne = \frac{P}{\rho \cdot d^5 \cdot n^3} \quad (1)$$

$$Re = \frac{\rho \cdot d^2 \cdot n}{\eta} \quad (2)$$

$$Q = \frac{\dot{\gamma}}{n} \quad (3)$$

For a Newtonian fluid, the dimensionless relationship $Ne = f(Re)$ is known. For a shear-thinning fluid, this equation can be expanded by Q , which results from extending the dimensional analysis for Newtonian fluids with the shear rate $\dot{\gamma}$. The product of Re and Q with the replacement of the shear velocity by

$$\eta = \frac{\tau}{\dot{\gamma}} \quad (4)$$

results in the Hedström number He (Eq. (5)).

$$He = \frac{\rho \cdot d^2 \cdot \tau}{\eta^2} \quad (5)$$

Keeping the Hedström number equal with $\tau = \text{const.}$ in the original and model, the function $Ne = f(Re)$ has the same shape at different scales [19]. Also, the density ρ is assumed to be constant in the original and model.

This approach achieves equal flow fields at different scales. The mixing time at different scales can be calculated via Eq. (6).

$$\frac{t_m}{t_o} = \frac{D_m}{D_o} \sqrt{\frac{\rho_o}{\rho_m}} \quad (6)$$

The similarity in the velocity fields is shown via equal normalized mixing times [18].

2.2 PIV Measurements

PIV is an optical measurement method to derive velocity vector fields in fluid flow experiments. Particles (here: polyamide (PA) particles, 55 μm) with similar density to the transparent model fluid are used as flow tracers to scatter the light of a line-laser (here: double-pulse Nd:YAG laser Litron Bernoulli 200-15 and laser light guiding arm) in the area of interest. Orthogonal to the light sheet, a camera (here: sCMOS camera with an objective Nikon AF Nikkor 28 mm $f/2.8D$) records the scattered light in double-frame pictures with a time-known distance. Using a geometric calibration, a velocity vector field is calculated for the area of interest [20].

3 Experiment

The experiment built for this work was designed according to the scale-up strategy of Annas et al. [18]. In Tabs. S1, S2, and S3 of the Supporting Information the values for the original and the scaled-down experiments for the three different types of agitators are given.

3.1 Test Rig

The experimental setup for this study consists of a two-chamber, transparent model container out of polymethylmethacrylate (PMMA). The agitator position and installation angle are presented in Fig. 1, along with the filling level for each setting. In the top view of the digester, the installation angle of each agitator is indicated. The center axes of the propeller and paddle agitator are aligned in parallel to the horizontal layer, whereas the long axis agitator is installed with an angle of 42° . The inner cylinder of the digester is scaled according to an original biogas digester with two propeller agitators. The outer area surrounded by a hexagonal wall is filled with model fluid to avoid heavy optical refraction of the laser light when entering the experiment and prevent distortion of the recorded pictures for vertical measurements.

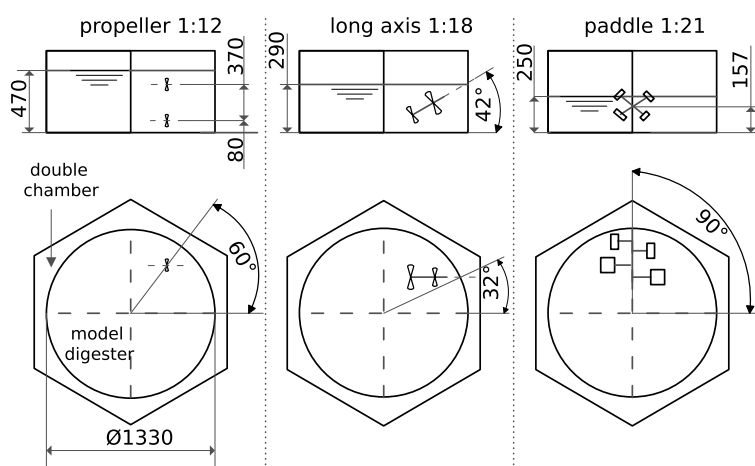


Figure 1. Schematic drawing of the scaled-down model digester with the propeller, long-axis, and paddle agitator.

Tab.2 lists the measurement layers for each setting. Four horizontal measuring layers have been investigated for the propeller, three for the long-axis agitator, and three for the paddle agitator.

Table 2. Height of measurement layers for different agitators.

	Propeller	Long axis	Paddle	Unit
Filling level	470	290	250	mm
4 th layer	440	–	–	mm
3 rd layer	320	240	200	mm
2 nd layer	200	160	140	mm
1 st layer	80	80	80	mm

3.2 Fluid Modeling

The model fluid consists of a CMC/water mixture. This substance was previously identified as an appropriate thickener fluid due to its transparency and the ability to approach the viscosity curve of the real digester content when mixed in the appropriate concentration [21]. The shear rate range from 10 to 1000 s⁻¹ can be approximated by the power law of Ostwald and de Waele (Eq. (7)) with a high coefficient of determination $R^2 = 0.99$ (Fig. S3).

$$\eta = k \cdot \dot{\gamma}^{m-1} \quad (7)$$

The blue line in Fig. 2 indicates the average dynamic viscosity depending on the mean shear rate calculated from various publications for the consistency index k and the flow index m for a DM content of 8% in the original digester. In contrast, the red line shows the wanted viscosity curve for a 1:12 scaled-down biogas digester mixed by a propeller agitator.

The considered publications and measurements for calculating average dynamic viscosity can be found in Tab. 3. The gray

shaded lines in Fig. 2 indicate the viscosity curves for various CMC/water mixtures. These are measured with the rheometer MCR 300 from Anton Paar GmbH using the cone-plate setup CP 50-1 with a cone angle of 1° and a cone diameter of 50 mm at a constant temperature of 20 °C.

The apparent viscosity (Eq. (9)) near the agitator is then calculated with an estimation for the shear rate (Eq. (8)) from Nguyen et al. [26]. In this work, the estimation of the shear rate for calculating the apparent viscosity for a non-Newtonian fluid is considered for a pipe flow. This approach is also used here to estimate the shear rate near the propeller. Eqs. (8) and (9) represent the equations for estimating the shear rate and apparent viscosity in an annular element around the vena contracta of a propeller mixer.

$$\dot{\gamma} = \frac{8 \cdot \bar{u}}{d} \quad (8)$$

$$\eta_a = k \cdot \left(\frac{8 \cdot \bar{u}}{d} \right)^{m-1} \quad (9)$$

Therefore, the average flow velocity in an annular element around the vena contracta is calculated according to ISO 21630 [27] for the propeller and long-axis agitator. As for the paddle agitator no common calculation rule for the average velocity around the agitator is known, 50% of the paddle tip speed is assumed to be the average flow velocity near the agitator.

Estimating the shear rate is essential to calculate the crucial ratio of shear rate to rotational speed (Eq. (3)) in the area of the agitator, also known as the Metzner-Otto constant [28, 29]. The Metzner-Otto constant is known for various agitator geometries for laminar flow. These values might also be appropriate for the transition area from laminar to turbulent flow ($Re_{\text{eff}} = 10$ to 10^4) [29]. The calculated Metzner-Otto constants for the agitators used in this study are in the range of the values given by Kraume et al. [29] for similar types of agitators. Nevertheless, it is pointed out that the approach of Metzner-Otto can only provide a rough estimation for the effective shear rate here [19].

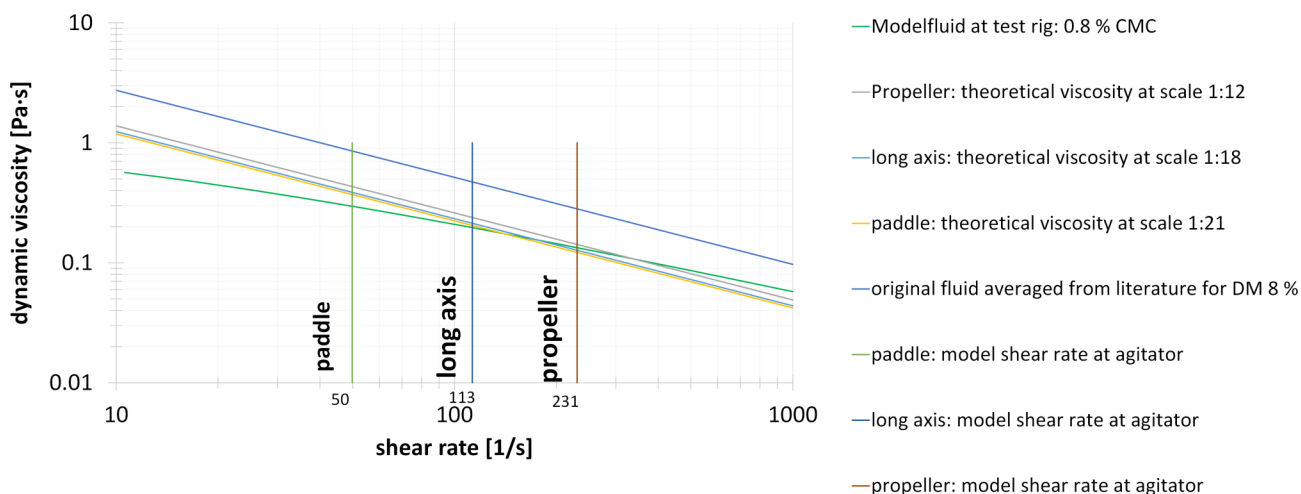


Figure 2. Dynamic viscosity depending on the shear rate for different CMC/water mixtures in the range of the power law approximation by Ostwald and de Waele.

Table 3. Power law parameters for dynamic viscosity approximation for measurements of digester content with around 8 % dry matter content.

Consistency index k [Pa s ⁻¹]	Flow index m [-]	DM content [%]	Measuring temp. [°C]	Comments	Ref.
14.32	0.209	7.28	40	Vane-Method [22]	[23]
21.58	0.43	8.22	40		
18.48	0.272	8.05	21	Pipe viscosimeter ($d = 43.2$ mm)	[24]
16.77	0.1998	7.64	39	Pipe viscosimeter (DN = 25, DN = 32, DN = 50, DN = 150)	[25]
16.26	0.1755	7.66	39		
12.43	0.3751	8.84	39		
8.331	0.3129	8.9	-		
8.372	0.2209	7.33	-		
14.567875	0.2744	7.99		Average values calculated from the literature mentioned above	

The estimated shear rates around the agitators in the model digester are in the range of the power law area. Tab. 4 shows the resulting Metzner-Otto constants based on the estimation of the average flow velocity near the agitator and using the shear rate estimation formula (Eq. (8)). Knowing the apparent viscosity (Eq. (9)) the effective Reynolds number Re_{eff} for the agitator region is derived. For the used agitators in this study, Re_{eff} is in the transition region from laminar to turbulent. Re_{eff} of the paddle agitator is in the same order of magnitude as the Re_{eff} for the paddle agitator analyzed in [18] (Tab. 4).

From all investigated mixtures, it was found that the line for 0.8 % CMC in Fig. 2 best meets the requirements on the dynamic viscosity for the 1:12 experiment with the propeller agitator for a DM content of 8 % according to the literature

data in Tab. 3. However, measurements of the prepared model fluid used in this experiment show a slight deviation from the wanted viscosity curve (Figs. S2 and S3). Consequently, the scaled rotational speed of the agitator needs to be recalculated with the measured viscosity parameters for the model fluid.

Therefore, the ratio Q (Eq. (3)), together with the power law for a non-Newtonian fluid by Ostwald and de Waele (Eq. (7)), is inserted in the Hedström number He to calculate the scaled rotational speed for the model digester.

$$n_M = \left[n_O^{2-m_O} \cdot \frac{k_M}{k_O} \cdot Q^{m_M-m_O} \cdot \frac{\rho_O \cdot D_O^2}{\rho_M \cdot D_M^2} \right]^{\frac{1}{2-m_M}} \quad (10)$$

Table 4. Estimated average shear rate around agitator, resulting Metzner-Otto constant, and comparison to literature data.

	Propeller	Long-axis agitator	Paddle agitator
Mean flow velocity at agitator region $ \bar{u} $ [m s ⁻¹]	2.4 ^{d)}	2.26 ^{d)}	1.5 ^{e)}
Scale	1:12	1:18	1:21
n_o [min ⁻¹]	153	38	12
n_m [min ⁻¹]	1726	629	214
$\dot{\gamma}_o$ [s ⁻¹]	20.42	6.82	2.79
$\dot{\gamma}_m$ [s ⁻¹]	231	113	50
Resulting Metzner-Otto constant Q [-]	8.01	10.77	11.96
Metzner-Otto constant Q from literature for a similar type of agitator [-]	10 ^{a)}	10 ^{a)}	13.95 ^{b)}
Re_{eff} [-]	1325	1181	599
Re_{eff} [-] from literature for a similar type agitator and fluid properties			336 ^{c)}

^{a)} Propeller agitator in [29]; ^{b)} inclined-bladed agitator in [29]; ^{c)} paddle agitator in CFD simulation [18]; ^{d)} derived from ISO 21630 [27]; ^{e)} estimated 50 % from paddle tip speed.

3.3 Procedure of Experiments

For measuring the velocity fields in the horizontal layers of the mixed model digester via PIV, the agitator (brushless DC motor from Oriental Motors GmbH (BLM5300HP-AS)) is started and run for a few minutes to achieve a stationary fluid flow.

Due to the camera's limited field of view and the container's relatively big cross section ($d = 1330$ mm), the model digester is split into four quadrants for the measurements. The area of interest is illuminated, and recordings are taken every 5 s for 10 min. This results in 120 double-frame pictures for one measurement in a quadrant, which are calculated to an average velocity field in the software DaVis10. The time difference between two frames is 20 ms. Four quadrants must be measured separately and stitched together to complete a flow field in one horizontal layer in the digester. The camera distance to the measuring layer is about 1.5 m (Fig. 3). Recording is done through the bottom of the model digester to avoid disturbance by light reflections of waves on the liquid surface.

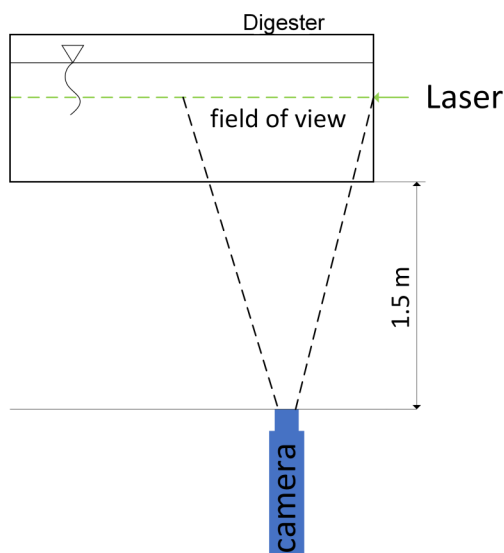


Figure 3. Scheme of the experiment: PIV measurement of a quadrant in a horizontal layer of the digester with a camera from the bottom.

4 PIV Measurement Results

Following up, relevant measurement results for the three different agitator settings are shown. The 2D flow fields are averaged over 10 min for the propeller, long-axis agitator, and paddle agitator in different horizontal layers and presented for the nominal rotational speeds in Figs. 4, 5, and 6. The nominal rotational speed is the rotational speed at the real plant applied to the model digester using the dimensional analysis. The color scale ranges from 0 to 0.4 m s^{-1} for each picture.

Horizontal layer's stitched velocity fields show certain discontinuities at some connection areas between the quadrants. This effect occurs because the measurements in the four quadrants are made one after the other and not simultaneously. Averaging over 10 min is not enough to get a continuous

connection between the velocity fields of the quadrants for the most turbulent areas.

2D PIV measurements only show the velocity vectors in the plane of interest. Turbulent flow is three-dimensional and instationary. Especially in the quadrants where the agitators are positioned, strong vertical velocity components are present, which are not captured by this measuring equipment. These areas close to the agitators have been masked out to suggest appropriate sensor positions.

Another restriction in the comparison of the measured velocity fields to the ones from the real plant comes from the difference between the model and original fluids. For example, there are no particles or fibers present in the model fluid used here, which might have an influence on the flow field [7]. Furthermore, the camera and laser beam were positioned manually, which contains a certain risk of failure.

4.1 Propeller Agitator

The average velocity fields of four horizontal measurement layers are depicted in Fig. 4 for the propeller agitator at the height of 80 mm above the reactor bottom (Fig. 1) and a nominal rotational speed of 1750 min^{-1} , which corresponds approximately to the rotational speed of 155 min^{-1} at the real plant.

The viscosity for this experiment is modeled with a 0.8 % CMC/water mixture and represents a viscosity of approximately 8 % DM content according to the formed mean value for viscosity out of various publications (Tab. 3). The four flow fields show a similar share around 60 % of the measurement layer which is moved with a horizontal velocity $> 0.05 \text{ m s}^{-1}$. Considering the propeller position, one can see the expected high flow velocities in measurement layer E080 towards the digester wall (Fig. 4a). Near the propeller, very low horizontal velocities are measured. Due to the highly turbulent flow in this region, one can assume that a high flow velocity is present, but it cannot be measured with the 2D PIV equipment in the horizontal layer. At the digester wall, the flow stream is guided along the wall and upwards towards the liquid filling level inside the digester. This can be seen in the relatively big area of high velocities in layer E440 (Fig. 4d).

In the real plant, a second propeller agitator is installed to mix the second half of the digester. Here, only the flow pattern of one propeller is investigated to find sensor positions that monitor the influence of the corresponding agitator.

4.2 Long-Axis Agitator

The long-axis agitator is installed with a vertical angle (Fig. 1). The material is sucked from the top of the liquid level and pumped towards the bottom of the digester. Fig. 5 shows the mean velocity fields in three different measurement layers for the nominal rotational speed of 700 min^{-1} , corresponding to 42 min^{-1} at the real plant. The experiment used the 0.8 % CMC/water mixture to model a DM content of 8 % (Tab. 3).

As the flow near the agitator blades is quite turbulent, and the agitator sucks material from top to bottom at a vertical angle, the blue areas indicating low flow velocities in the velo-

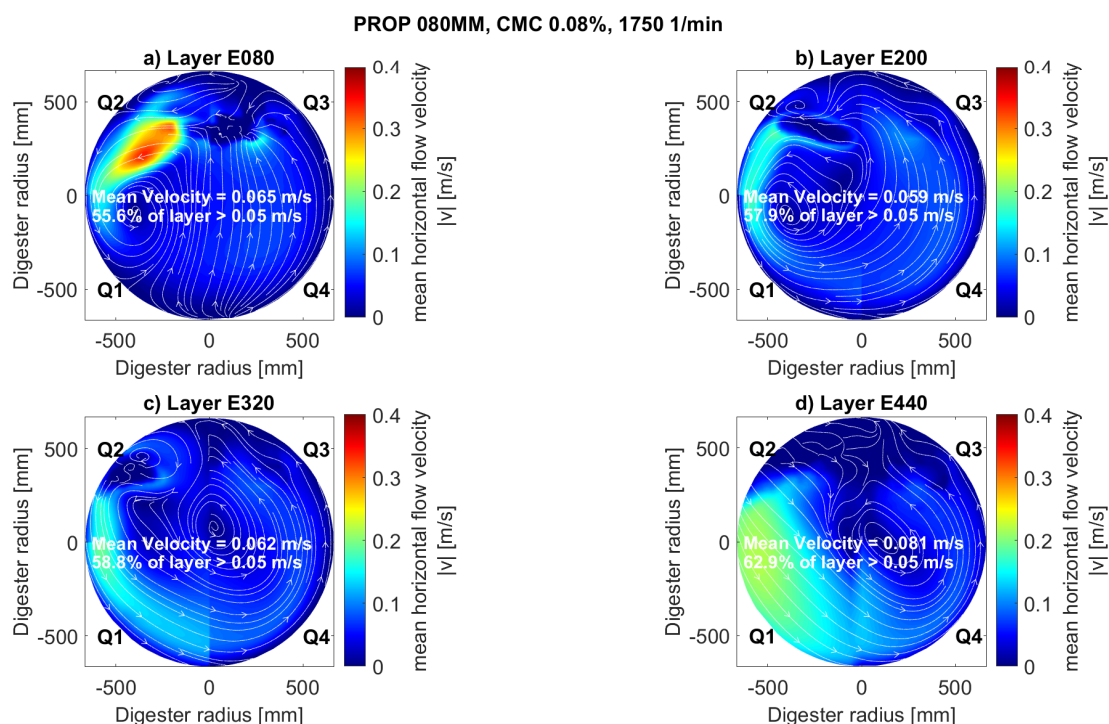


Figure 4. Flow fields: propeller at 80 mm distance from bottom, 1750 min^{-1} , and different measurement layers (80, 200, 320, 440 mm from bottom) labeled E080, E200, E320, E440. CMC/water mixture: 0.8 %.

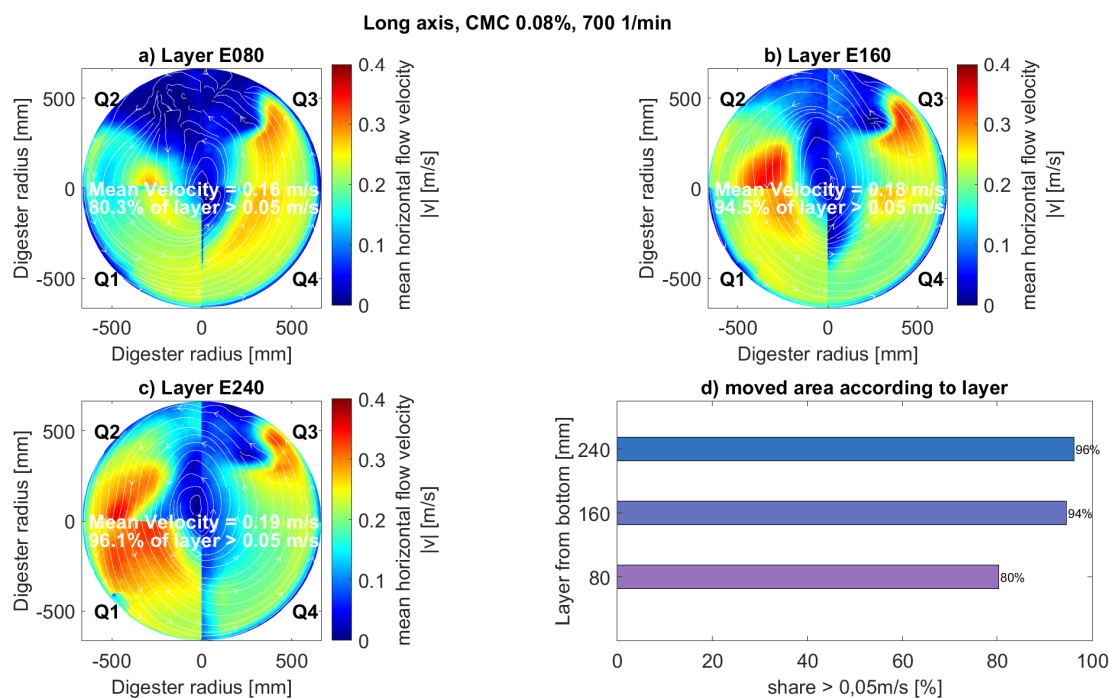


Figure 5. Flow fields: long axis, 700 min^{-1} , and different measurement layers (80, 160, 240 mm from bottom) labeled E080, E160, E240. CMC/water mixture: 0.8 %.

city fields of Fig. 5 do not necessarily mean that there is no movement. It indicates that low flow velocities are measured in the horizontal measurement layer with the 2D PIV equipment.

Fig. 5d shows a bar diagram with the share of the measurement area moved above 0.05 m s^{-1} on the x -axis and the measurement layers from the bottom on the y -axis. Shares of

measurement layers moved above the critical velocity of 0.05 m s^{-1} of greater than 80 % can be observed.

In the real plant, an additional propeller agitator is located in quadrant Q1. Also, here, only the influence of the long-axis agitator is investigated to find positions for monitoring it.

4.3 Paddle Agitator

The paddle agitator is located 157 mm above the ground in the model digester (Fig. 1). That is related to 3.3 m in the real plant. Fig. 6 shows the mean velocity fields for three different measurement layers. A rotational speed of 250 min^{-1} complies with 14 min^{-1} in the real plant. The 0.8 % CMC/water mixture is used. Fig. 6d shows the share of measurement layer moved above 0.05 m s^{-1} . For all three measurement layers, this share is around 50 %. In the real plant, a second paddle agitator would be in charge of the second half of the digester. The flow pattern in the central measurement layer E140 displays an axial suction stream towards the agitator and radial release (Fig. 6b).

4.4 Data Analysis – Finding Relevant Positions for the Implementation of Flow Sensors

The target parameter for finding possibly appropriate positions for the flow sensor on the circumference of the digester is the geometric angle on a circle 60 mm smaller in diameter than the outer diameter of the model digester in a specific horizontal measurement layer (Fig. 7). This should overcome the influence of the boundary layer at the wall. The positioning strategy for a

flow sensor is explained by the example of the propeller agitator (Fig. 7).

As a critical flow velocity, this work sticks to the recommendation by Jobst et al. [15] of 0.05 m s^{-1} . The percentage of the measurement layer moved above 0.05 m s^{-1} – later referred to as “share $> 0.05 \text{ m s}^{-1}$ ” – is the wanted target parameter. It should be estimated via a local flow speed measurement on the evaluation circle. An installation angle for a flow speed sensor on the evaluation circle is searched. Therefore, the correlation coefficient of flow velocity and share $> 0.05 \text{ m s}^{-1}$ is calculated for each angle position on the evaluation circle. Additionally, the maximum to minimum flow velocity difference is derived for each angle position on the evaluation circle. Finally, velocity difference and correlation coefficient are normed and multiplied to get a position factor. Based on the maximum position factor, an optimum installation angle for each agitator and installation layer can be defined to estimate the share $> 0.05 \text{ m s}^{-1}$.

Therefore, the velocity is read out on the defined evaluation circle (Fig. 7) from 0 to 360° in 1° -steps in a certain measurement layer. The following pseudo-code implemented in Matlab R2020a shows how the suggested sensor position is found for monitoring the propeller agitator:

```

FOR each angle on the evaluation circle in a measurement layer
  Get velocity for each parameter setting.
  Get share  $> 0.05 \text{ m s}^{-1}$  for each parameter setting.
  Calculate the correlation coefficient of velocity and share  $> 0.05 \text{ m s}^{-1}$  and normalize it.
  Calculate the velocity difference from maximum to minimum and normalize it.
  position factor = normed correlation coefficient * normed velocity difference.
END FOR
  
```

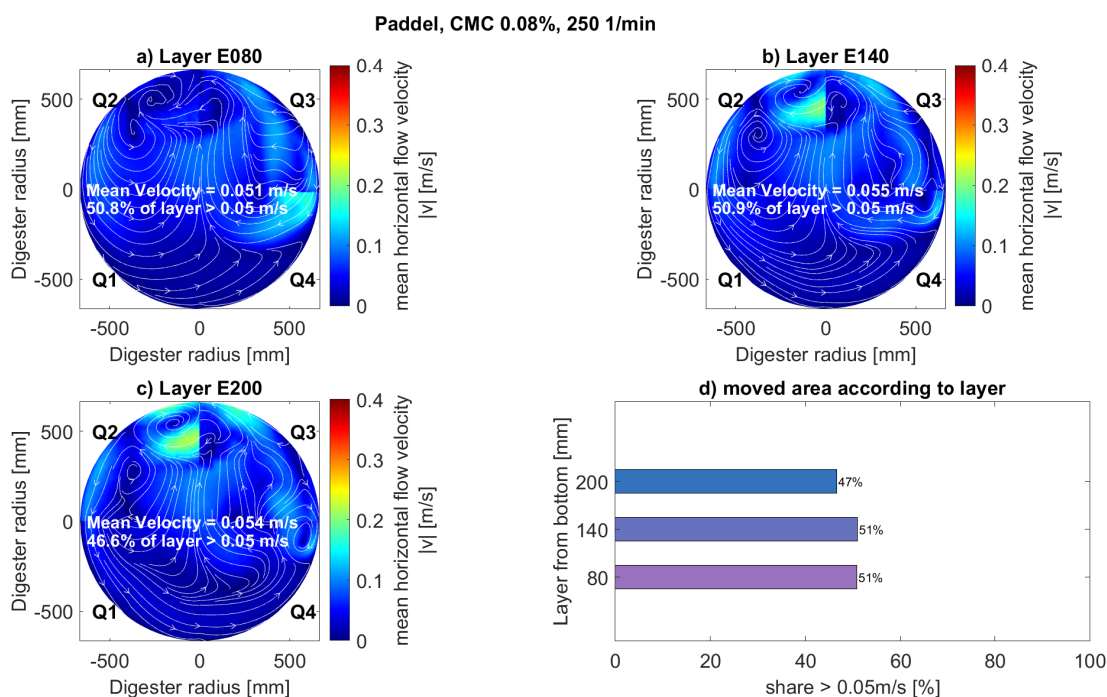


Figure 6. Flow fields: paddle agitator, 250 min^{-1} , and different measurement layers (80, 140, 200 mm from bottom) labeled E080, E140, E200. CMC/water mixture: 0.8 %.

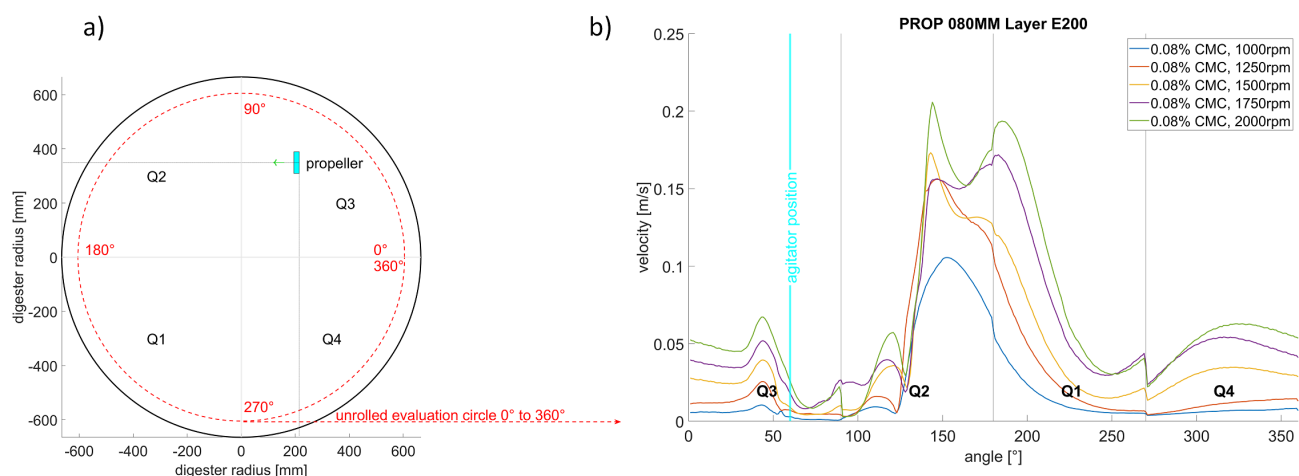


Figure 7. (a) Evaluation circle (red dashed line); (b) average horizontal velocity magnitude on evaluation circle.

Set mask: define the area of interest for a sensor position by setting minimum and maximum angle
 installation position = max (position factor in the area of interest)

Following this approach, positions with high correlations of a local flow speed measurement to a global quantity like share $> 0.05 \text{ m s}^{-1}$ are found. Additionally, considering the velocity difference at the measurement position and calculating the position factor ensures optimum measurability.

Fig. 8a indicates sensor position $\alpha_{\text{sensor}} = 192^\circ$ by a green vertical line for the measurement layer E200 based on the maximum of the position factor.

the share $> 0.05 \text{ m s}^{-1}$ at $\alpha_{\text{sensor}} = 192^\circ$ with a coefficient of determination $R^2 = 0.98$ is shown in Fig. 8b. This result is derived when using a mixture of 0.8 % CMC at five different rotational speeds. The correlation of velocity and share $> 0.05 \text{ m s}^{-1}$ is quite high for a large area around this measurement layer's circumference. However, the correlation drops a lot from the agitator position to about 150° , where it starts increasing. A reason for that is the turbulent flow near the propeller. Only the area from 150° to 360° is considered for a possible sensor position.

The velocity profile on the evaluation circle looks quite different for the long-axis and paddle agitators, as expected from

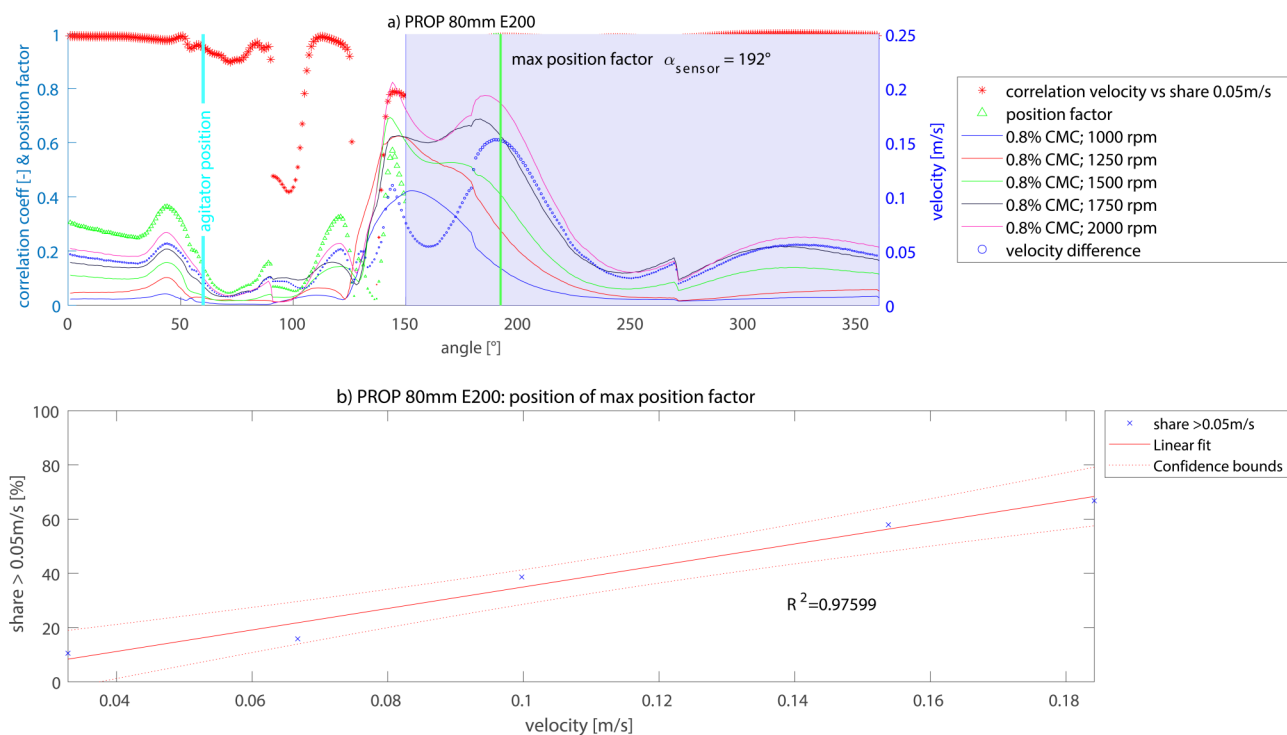


Figure 8. Propeller agitator 80 mm from the bottom. (a) Indication of sensor position angle α_{sensor} in layer E200; (b) linear fit of velocity and share $> 0.05 \text{ m s}^{-1}$ at α_{sensor} .

their geometry and installation position. Moreover, two different CMC/water mixtures have been measured and included in the data analysis for these two agitators. This delivers optimum sensor positions also for an increase in fluid viscosity. The correlation coefficient for the paddle agitator appears to vary around the evaluation circle more than for the long-axis agitator (Figs. 9 and 10). That means an appropriate position for placing a local flow speed measurement device for predicting the global mixing quality criteria share $> 0.05 \text{ m s}^{-1}$ has to be chosen even more carefully.

In Tab. 5, a summary of performed experiments is shown with the resulting angle for the sensor position. The measurement layers which result in the highest coefficient of determination R^2 are marked in bold letters.

In future works, a wider parameter study can be performed by validated CFD simulations to increase the database and refine the results of the sensor positions. To enhance the coefficient of determination R^2 for the long-axis and paddle agitators, a second sensor position could be considered. Subsequently, experiments at real plants are required to test the proposals for the sensor positions.

5 Conclusion

A method for positioning flow velocity sensors to monitor agitators in agricultural biogas digesters with optimum correlation to a global flow field parameter is presented. Flow fields of a propeller, a long-axis and a paddle agitator are measured in a PIV test rig using a CMC/water mixture as a model fluid.

The similarity of measured flow fields in the experiment to the real digesters is ensured by an equal Hedström number in the model and original, leading to scaled geometry, rotational speed, and viscosity parameters. Applying this dimensional analysis, the resulting angles for the sensor positions conform directly to the real plant.

PIV measurements are performed in various horizontal layers at different rotational speeds and viscosities. In evaluating the PIV measurements, a position factor is defined considering the correlation of a local flow velocity sensor to a global flow field parameter and the velocity range at the measurement position. At the maximum of the position factor, the optimum sensor position is found.

These suggestions are made to avoid positioning the flow sensors in dead zones or too close to the agitators to ensure high correlation coefficients between local flow velocity measurement and a global flow field parameter. Although their flow fields differ significantly, the presented method can be applied to all three agitators.

Supporting Information

Supporting Information for this article can be found under DOI: <https://doi.org/10.1002/ceat.202300241>.

Data Availability Statement

The data that support the findings of this study are available from the corresponding author upon reasonable request.

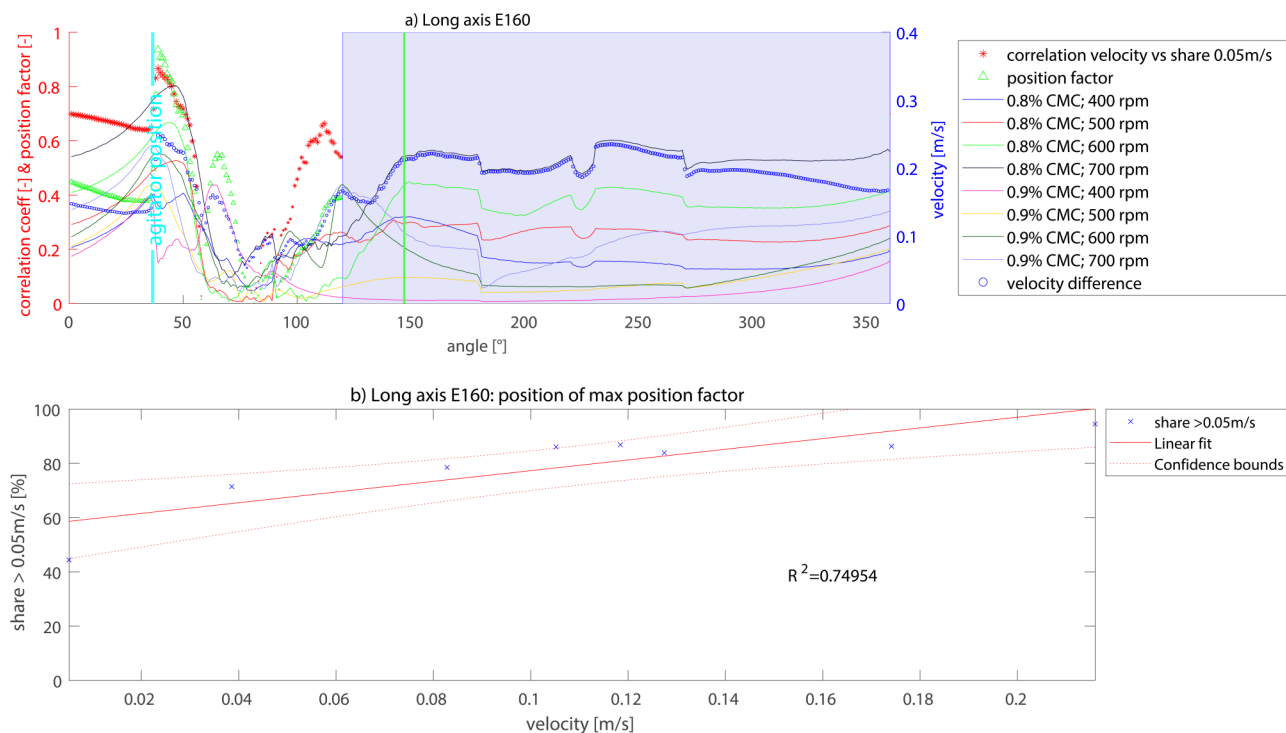


Figure 9. Long-axis agitator. (a) Velocity profile on evaluation circle with an indication of sensor position angle α_{sensor} based on the position factor maximum; (b) linear fit of velocity and share $> 0.05 \text{ m s}^{-1}$ at α_{sensor} .

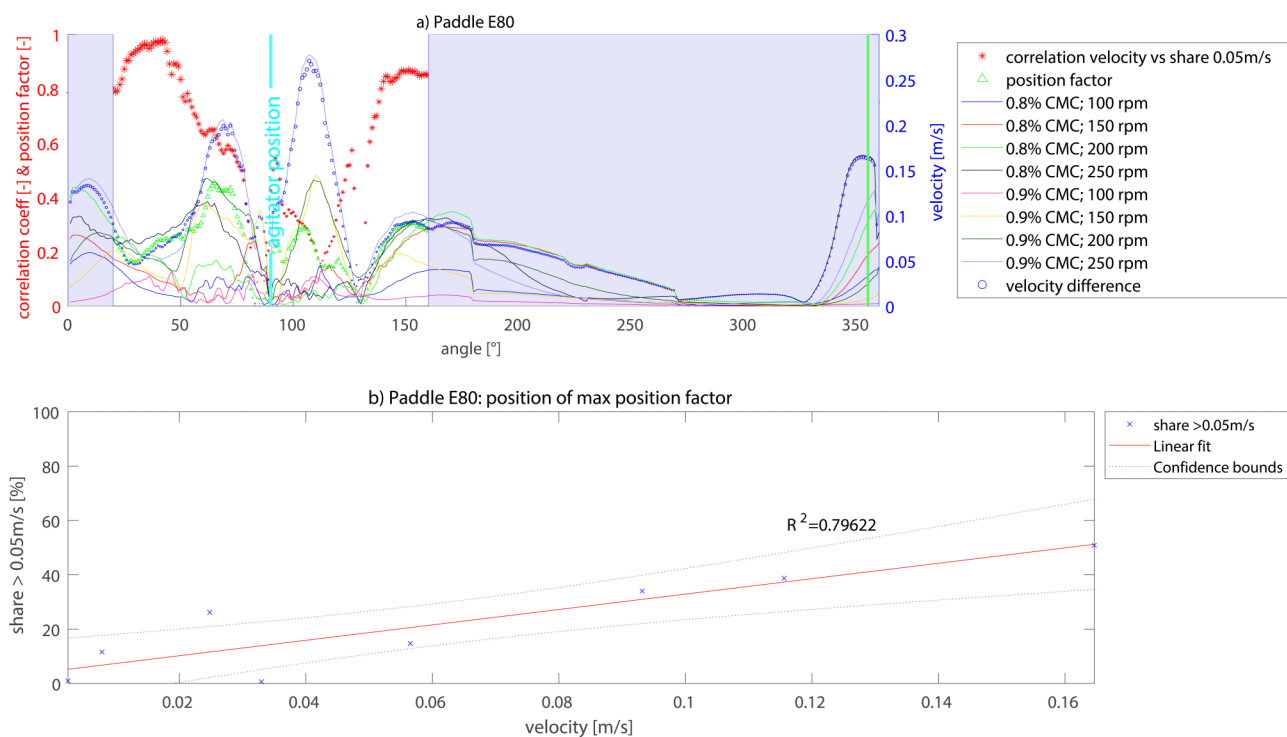


Figure 10. Paddle agitator. (a) Velocity profile on evaluation circle with an indication of sensor position angle α_{sensor} based on the position factor maximum; (b) linear fit of velocity and share $> 0.05 \text{ m s}^{-1}$ at α_{sensor} .

Table 5. Summary of performed experiments.

Agitator	Number of layers	rpm	Number of viscosities	Measurement layer	Angle sensor position [°]	Position factor	R^2	Seeding
Propeller 80mm ^{a)}	4	5	1	80	180	0.95	0.91	PA particles 55 μm
				200	192	0.99	0.98	
				320	194	1.00	0.99	
				440 ^{c)}	161	0.95	1.00	
Propeller 370mm ^{b)}	4	5	1	80	182	0.99	0.95	PA particles 55 μm
				200 ^{c)}	171	0.98	0.96	
				320	162	0.91	0.92	
				440	161	0.56	0.67	
Long axis	3	4	2	80	264	0.80	0.51	Air bubbles
				160 ^{c)}	147	0.80	0.75	
				240	158	0.74	0.64	
Paddle	3	4	2	80 ^{c)}	355	0.55	0.80	Air bubbles
				140	348	0.42	0.70	
				200	165	0.34	0.41	

^{a)} Propeller at 80 mm installation height from the bottom; ^{b)} propeller at 370 mm installation height from the bottom; ^{c)} measurement layer, which results in the highest R^2 for the linear fit of velocity and share $> 0.05 \text{ m s}^{-1}$ at the defined angle for the sensor position.

Acknowledgment

The authors are very grateful for the financial support of the Dobeneck-Technologie-Stiftung, who enabled the construction of the experiment and the investment in a 2D PIV System. Many thanks also go to the Technologie- und Förderzentrum for the advice and construction of mechanical components. Open access funding enabled and organized by Projekt DEAL.

The authors have declared no conflict of interest.

Symbols used

d	[m]	diameter of the stirrer
D	[m]	diameter of the digester
He	[-]	Hedström number
k	[Pa s ⁻¹]	consistency index
m	[-]	flow index
n	[s ⁻¹]	rotational speed
Ne	[-]	Newton number
P	[W]	stirring power
Q	[-]	ratio of shear rate to rotational speed
Re	[-]	Reynolds number
Re_{eff}	[-]	effective Reynolds number
t	[s]	mixing time
\bar{u}	[m s ⁻¹]	average estimated flow velocity near the impeller
v	[m s ⁻¹]	flow velocity

Greek letters

α	[°]	positioning angle for a flow sensor
$\dot{\gamma}$	[s ⁻¹]	shear rate
η	[kg m ⁻¹ s ⁻¹]	dynamic viscosity
ρ	[kg m ⁻³]	density
τ	[N mm ⁻²]	shear stress

Sub- and Superscripts

app	apparent
m	model
o	original

Abbreviations

BMP III	Biogas-Messprogramm III
CFD	computational fluid dynamics
CMC	carboxymethyl cellulose
CSTR	continuously stirred tank reactor
DM	dry matter
FNR	Fachagentur Nachwachsende Rohstoffe e. V.
PA	polyamide
PIV	particle image velocimetry
PMMA	polymethylmethacrylate

References

- [1] Bundesamt für Justiz, Bundes-Klimaschutzgesetz (KSG) **2019**. <https://www.gesetze-im-internet.de/ksg/BjNR251310019.html> (Accessed on June 14, 2023)
- [2] M. Maciejczyk, *Biogasindustryfigures* **2021**, <https://www.biogas.org/edcom/webfvb.nsf/id/en-german-biogas-market-data> (Accessed on November 30, 2021)
- [3] P. Weiland, *Appl. Microbiol. Biotechnol.* **2010**, *85* (4), 849–860. DOI: <https://doi.org/10.1007/s00253-009-2246-7>
- [4] Fachagentur Nachwachsende Rohstoffe e. V., FNR – Biogas: Faustzahlen, <https://biogas.fnr.de/daten-und-fakten/faustzahlen> (Accessed on May 16, 2022)
- [5] G. Dachs, W. Rehm, *Der Eigenstromverbrauch von Biogasanlagen und Potenziale zu dessen Reduzierung* **2006**, https://www.infothek-biomasse.ch/images/2006_SOLARENE-FOERDERVER_Eigenstromverbrauch_Biogasanlagen.pdf (Accessed August 3, 2023)
- [6] F. Conti, L. Wiedemann, M. Sonnleitner, A. Saidi, M. Goldbrunner, *Renewable Energy* **2019**, *132*, 351–362. DOI: <https://doi.org/10.1016/j.renene.2018.08.013>
- [7] A. Lomtscher, K. Jobst, S. Fogel, K. Rostalski, S. Stempin, M. Kraume, *Flow Meas. Instrum.* **2017**, *53*, 56–66. DOI: <https://doi.org/10.1016/j.flowmeasinst.2016.10.002>
- [8] L. Li, K. Wang, Q. Zhao, Q. Gao, H. Zhou, J. Jiang, W. Mei, *Rev. Environ. Sci. Biotechnol* **2022**, *21* (3), 665–689. DOI: <https://doi.org/10.1007/s11157-022-09626-z>
- [9] E. Witkowska, A. Buczkowska, A. Zamojska, K. W. Szewczyk, P. Ciosek, *Bioresour. Technol.* **2010**, *80* (1), 87–93. DOI: <https://doi.org/10.1016/j.biotech.2010.08.004>
- [10] M. Mönch-Tegeder, A. Lemmer, J. Hinrichs, H. Oechsner, *Bioresour. Technol.* **2015**, *178*, 278–284. DOI: <https://doi.org/10.1016/j.biortech.2014.08.041>
- [11] A. Nsair, O. Bade, K. Kuchta, *Environ. Res. Technol.* **2018**, *1*, 51–56.
- [12] P. Kress, H.-J. Nägele, A. Lemmer, B. Kolb, in press. DOI: <https://doi.org/10.1515/LT.2020.3230>
- [13] L. Weber, S. Annas, G. Messing, M. Elfering, H.-A. Jantzen, J. Scholz, in *Biogas in der Landwirtschaft – Stand und Perspektiven*, Kuratorium für Technik und Bauwesen in der Landwirtschaft e. V. (KTBL), Darmstadt **2021**.
- [14] L. Buntkiel, C. Budelmann, A. Heller, S. Annas, S. Reinecke, U. Hampel, in *Biogas in der Landwirtschaft – Stand und Perspektiven*, Kuratorium für Technik und Bauwesen in der Landwirtschaft e. V. (KTBL), Darmstadt **2021**.
- [15] K. Jobst, A. Lomtscher, A. Deutschmann, S. Fogel, K. Rostalski, S. Stempin, M. Brehmer, M. Kraume, in *Biogas in der Landwirtschaft: Stand und Perspektiven*, FNR/KTBL-Online-Kongress, Potsdam, KTBL-Schrift, Vol. 508, Kuratorium für Technik und Bauwesen in der Landwirtschaft e. V. (KTBL), Darmstadt **2015**.
- [16] Fachagentur Nachwachsende Rohstoffe e. V., *Biogas-Messprogramm III*, Fachagentur Nachwachsende Rohstoffe e. V. (FNR), Gülzow-Prüzen **2021**.
- [17] J. C. Gibbins, *Dimensional Analysis*, Springer, London **2011**.
- [18] S. Annas, H.-A. Jantzen, J. Scholz, U. Janoske, *Chem. Eng. Technol.* **2018**, *41* (4), 739–746. DOI: <https://doi.org/10.1002/ceat.201700447>

- [19] G. Böhme, M. Stenger, *Chem. Eng. Technol.* **1988**, *11* (1), 199–205. DOI: <https://doi.org/10.1002/ceat.270110127>
- [20] *Particle Image Velocimetry: A Practical Guide*, 3rd ed. (Eds: M. Raffel, C. E. Willert, F. Scarano, C. J. Kähler, S. T. Wereley, J. Kompenhans), Springer International Publishing, Cham **2018**.
- [21] L. Wiedemann, F. Conti, T. Janus, M. Sonnleitner, W. Zörner, M. Goldbrunner, *Chem. Eng. Technol.* **2017**, *40* (2), 238–247. DOI: <https://doi.org/10.1002/ceat.201600194>
- [22] N. Q. Dzuy, D. V. Boger, *J. Rheol.* **1985**, *29* (3), 335–347. DOI: <https://doi.org/10.1122/1.549794>
- [23] Fraunhofer IKTS, TU Berlin, KSB GmbH & Co. KG, *Entwicklung eines Steuerungs- und Regelkonzeptes für Mischprozesse in Biogasfermentern auf der Basis zu validierender Prozessmodelle*. Schlussbericht Forschungsvorhaben **2017**, <https://www.fnr.de/ftp/pdf/berichte/22005913.pdf> (Accessed on August 3, 2023)
- [24] M. Brehmer, T. Eppinger, M. Kraume, *Chem. Ing. Tech.* **2012**, *84* (11), 2048–2056. DOI: <https://doi.org/10.1002/cite.201200062>
- [25] C. Koll, *Master Thesis*, Leibniz University, Hannover **2012**.
- [26] Q.-H. Nguyen, N.-D. Nguyen, in *Continuum Mechanics* (Ed: Y. X. Gan), IntechOpen, London **2012**.
- [27] ISO 21630:2007, *Pumps – Testing – Submersible mixers for wastewater and similar applications*, ISO, Geneva **2007**.
- [28] J. Wu, L. J. Graham, N. Noui Mehidi, *AIChE J.* **2006**, *52* (7), 2323–2332. DOI: <https://doi.org/10.1002/aic.10857>
- [29] M. Kraume, in *Handbuch der Geodäsie* (Eds: W. Freeden, R. Rummel), Springer, Berlin **2019**.